Role of Vitamin D Receptor in the Antiproliferative Effects of Calcitriol in Tumor-Derived Endothelial Cells and Tumor Angiogenesis *In vivo*

Ivy Chung,[1] Guangzhou Han,[1] Mukund Seshadri,[2] Bryan M. Gillard,[1] Wei-dong Yu,[1] Barbara A. Foster,[1] Donald L. Trump,[3] and Candace S. Johnson[1]

Departments of [1]Pharmacology and Therapeutics, [2]Cancer Biology, and [3]Medicine, Roswell Park Cancer Institute, Buffalo, New York

Abstract

Calcitriol (1,25-dihydroxycholecalciferol), the major active form of vitamin D, is antiproliferative in tumor cells and tumor-derived endothelial cells (TDEC). These actions of calcitriol are mediated at least in part by vitamin D receptor (VDR), which is expressed in many tissues including endothelial cells. To investigate the role of VDR in calcitriol effects on tumor vasculature, we established TRAMP-2 tumors subcutaneously into either VDR wild-type (WT) or knockout (KO) mice. Within 30 days post-inoculation, tumors in KO mice were larger than those in WT ($P < 0.001$). TDEC from WT expressed VDR and were able to transactivate a reporter gene whereas TDEC from KO mice were not. Treatment with calcitriol resulted in growth inhibition in TDEC expressing VDR. However, TDEC from KO mice were relatively resistant, suggesting that calcitriol-mediated growth inhibition on TDEC is VDR-dependent. Further analysis of the TRAMP-C2 tumor sections revealed that the vessels in KO mice were enlarged and had less pericyte coverage compared with WT ($P < 0.001$). Contrast-enhanced magnetic resonance imaging showed an increase in vascular volume of TRAMP tumors grown in VDR KO mice compared with WT mice ($P < 0.001$) and FITC-dextran permeability assay suggested a higher extent of vascular leakage in tumors from KO mice. Using ELISA and Western blot analysis, there was an increase of hypoxia-inducible factor-1α, vascular endothelial growth factor, angiopoietin 1, and platelet-derived growth factor-BB levels observed in tumors from KO mice. These results indicate that calcitriol-mediated antiproliferative effects on TDEC are VDR-dependent and loss of VDR can lead to abnormal tumor angiogenesis. [Cancer Res 2009;69(3):967–75]

Introduction

Calcitriol has effects on multiple tissues by regulating cell proliferation, differentiation, and apoptosis (1, 2). Calcitriol has profound antitumor activity in many *in vitro* and *in vivo* human and murine tumor models, including leukemia (3), squamous cell carcinoma (4), prostate (5), breast (6), and colon cancer (7). Calcitriol has antiproliferative effects not only on malignant epithelial cells (2), but also on endothelial cells freshly isolated from tumors [tumor-derived endothelial cells (TDEC); refs. 8, 9]. Treatment with calcitriol promotes G_0/G_1 cell cycle arrest and induces apoptosis in TDEC (9, 10). The growth inhibition observed in TDEC is accompanied by the modulation of cell cycle proteins (p21 and p27), down-regulation of survival markers (phosphorylated-Akt and phosphorylated-Erk), and increase in cleavage of caspase-3 and PARP (9).

The actions of calcitriol are mediated by the vitamin D receptor (VDR), a member of the nuclear receptor superfamily (11). VDR expression is observed in several endothelial cell types, including TDEC (9, 12, 13). Treatment with calcitriol induces the up-regulation of VDR protein expression, promotes receptor phosphorylation, and increases receptor trafficking into the nucleus in TDEC (9). Ligand-bound VDR heterodimerizes with the retinoid X receptor and interacts with specific DNA sequences to regulate gene expression (9, 14).

The physiologic consequences of calcitriol/VDR disruption have been investigated in animals and humans deficient in vitamin D as well as in those with VDR mutations (15–18). Defects in VDR structure, which impair the function of the receptor, are shown to be the molecular basis for the human vitamin D–resistant rickets (19, 20). The study of mice with targeted ablation of VDR has provided substantial insights into the role of the receptor in various calcitriol effects (11, 21–23). In the VDR knockout (KO) mice, VDR ablation seems to increase sensitivity to mammary gland tumorigenesis and chemical-induced skin carcinogenesis. Thus, supporting the role of vitamin D signaling in tumor development (6, 24). Whether VDR plays a major role in calcitriol-mediated antiproliferative effects on TDEC or tumor angiogenesis is unclear. Because formation of blood vessels in the tumor requires participation from the host cells (25, 26), in this study, we compared TDEC isolated from tumors derived from a cell line established from the transgenic adenocarcinoma of the mouse prostate model (TRAMP-C2) in VDR wild-type (WT) and KO mice. TRAMP cells express WT VDR but the endothelial cells recruited into the tumors will be determined by the hosts' genetic background.

Materials and Methods

Chemicals and Reagents

Calcitriol (Hoffmann-LaRoche) was reconstituted in 100% ethanol and stored, protected from light, under a layer of nitrogen gas at −70°C. All handling of calcitriol was performed with indirect lighting. Immediately prior to use, calcitriol was diluted to the final concentrations in tissue culture medium. For most applications, calcitriol was used at 10 nmol/L, a concentration that consistently shows antiproliferative effects in multiple assays in a variety of tumor cell types. Albumin-GdDTPA (courtesy of Robert Brasch) was obtained from Contrast Media Laboratory, Department of

Requests for reprints: Candace S. Johnson, Department of Pharmacology and Therapeutics, Roswell Park Cancer Institute, Elm and Carlton Streets, Buffalo, NY 14263. Phone: 716-845-8300; Fax: 716-845-1258; E-mail: Candace.Johnson@roswellpark.org.

doi:10.1158/0008-5472.CAN-08-2307

Radiology, University of California at San Francisco (San Francisco, CA). This agent has been extensively characterized and used for experimental studies (27).

Animal Models

A breeding colony of VDR KO mice was established from mice generously provided by Dr. Marie Demay (Harvard Medical School, Boston, MA). The phenotype of these mice, generated by targeted ablation of the second zinc finger of the DNA-binding domain of the VDR, resembles the human vitamin D–dependent rickets type II (11). Mice were genotyped by PCR amplification of DNA isolated from tail cuts using primers targeting exon 3 (second zinc finger region) for WT mice and the neomycin gene (replaces exon 3) for KO mice. All VDR KO and WT mice were fed with a diet containing 2% calcium, 1.25% phosphorus, and 20% lactose with 2.2 IU vitamin D_3/g (TD96348; Teklad). This diet has been shown to normalize serum mineral homeostasis, bone growth, and body weight in VDR KO mice (28). TRAMP C2 (TRAMP) cells were maintained in RPMI 1640 with 10% fetal bovine serum and 1% penicillin/streptomycin (29). TRAMP-2 cells (2×10^6) were inoculated s.c. in 0.1 mL HBSS/Matrigel (1:1) solution into age-matched VDR WT and KO male mice. Tumor growth was monitored over time and tumor size was measured using calipers. Tumor volumes were calculated by the following formula: volume = (length $\times$ width^2) / 2. After 31 days, tumors were harvested and processed for endothelial cell isolation, immunohistochemical, or molecular studies. All mice breeding and handling were approved by the Institutional Animal Care and Use Committee at Roswell Park Cancer Institute.

Isolation of TDEC

Isolation and identification of TDEC from TRAMP tumors implanted in VDR WT and KO mice were performed using procedures described previously (9, 30). TDEC were cultured on 1% gelatin-coated flasks (Corning Glass, Inc.) in DMEM/10% v/v fetal bovine serum/1% penicillin and streptomycin. For all experiments, endothelial cells used were at low passage (<8).

Immunohistochemistry

Endothelial CD31 staining. Tumors were excised and immediately placed in zinc fixative (BD Biosciences PharMingen) overnight, transferred to 70% ethanol, dehydrated, and embedded in paraffin. Sections 5 μm thick were stained after conventional deparaffinization, endogenous peroxidase quenching with 3% H_2O_2, and pretreatment with 0.03% casein in PBS with 500 μL/L of Tween for 30 min at room temperature to block nonspecific binding. Slides were counterstained with Harris hematoxylin (Poly Scientific). Mouse CD31 was detected with rat monoclonal antibody (IgG_{2a}; BD Biosciences PharMingen) at 1:50 dilution in PBS for 60 min at 37°C. This was followed by the addition of biotinylated rabbit anti-rat IgG (BD Biosciences PharMingen) at 1:100 dilution for 30 min, streptavidin peroxidase (Zymed) for 30 min, and diaminobenzidine for 5 min. An isotype-matched control (10 μg/mL rat IgG) was used on a duplicate slide in place of the primary antibody as a negative control.

CD31/α-smooth muscle actin double staining. Frozen sections (6 μm) were cut and stored at −80°C until the assay was run. The slides were thawed quickly and fixed for 10 min in cold acetone (−20°C). After blocking, α-smooth muscle actin (α-SMA) antibody was used at 1/250 for 30 min and was detected by biotinylated goat anti-rabbit secondary antibody 25 min followed by streptavidin peroxidase for an additional 25 min. 3,3′-Diaminobenzidine was used as the chromogen for α-SMA. After a second blocking step, sections were incubated with CD31 (BD Biosciences PharMingen) at 5 μg/mL for 30 min followed by biotinylated anti-rat secondary antibody for 25 min and alkaline phosphatase-conjugated streptavidin reagent for 25 min. The chromogen, Fast Red, was used to detect CD31. An isotype-matched control (2 μg/mL rabbit IgG and 5 μg/mL rat IgG) was used on a duplicate slide in place of the primary antibody as a negative control.

Vessel Morphologic Analysis

Mean vessel density. Intratumoral blood vessels were counted on cross-sections of tumors stained with endothelial cell marker CD31.Using a light microscope, images of five fields at consistent locations for each sample were taken at ×100 magnification. The average number of microvessels per field was calculated using Image J software (NIH, Bethesda, MD). Vessels with a clearly defined lumen or a well-defined linear vessel shape were counted. Single endothelial cells were not counted as vessels.

Vessel lumen area. Images of vessels at the locations described above were taken at high-power field (magnification, ×400). Vessel lumen area was determined using the software Analyze 7.0 (AnalyzeDirect), by measuring the vessel lumen circumference stained with CD31 antibody.

Pericyte coverage analysis. Images of vessels in sections stained with CD31 and α-SMA were taken at high-power field (magnification, ×400). CD31- and α-SMA–positive areas were measured for each vessel using Analyze 7.0 software. Pericyte coverage for each vessel was calculated using the formula: (CD31 and α-SMA overlapping area) / (total CD31 positive area).

Contrast-Enhanced Magnetic Resonance Imaging

Magnetic resonance imaging of tumor-bearing mice was carried out in a 4.7 T horizontal bore scanner (General Electric NMR Instruments). We have previously described the imaging protocol for calculating tumor vascular volume using the intravascular contrast agent, albumin-GbDTPA (27). Regional precontrast T_1 values were calculated from a series of three preliminary images acquired prior to contrast agent administration. Following these baseline acquisitions, albumin-GdDTPA (0.1 mmol/kg) was injected via tail vein and a second series of five post-contrast images was acquired for ~45 min, as described previously (27). Image processing and analysis were carried out using commercially available software (Analyze PC, version 7.0; AnalyzeDirect). Regions of interest of tumors, kidneys, and muscle tissues were manually drawn on the images and object maps of the regions of interest constructed. The longitudinal relaxation rate ($R_1 = 1/T_1$) for each region of interest was computed using MATLAB (version 7.0; Math Works, Inc.), and source codes were developed by RPCI Preclinical Imaging Resource. Linear regression analysis of the change in RI (ΔRI) over the 45 min period was used to compare vascular volume and permeability (27) and differences between tumors in WT ($n = 7$) and KO mice ($n = 8$) analyzed for statistical significance using Prism (version 5.00, GraphPad Prism).

In vivo Evans Blue Dye Assay

Mice received intracardiac injections of 200 μL of Evans blue dye (0.5%; Sigma) for 5 min while under anesthesia. After sacrifice, tumors and livers were collected and incubated with formamide (Fisher) at 55°C overnight. The amount of dye extracted from each sample was quantitated by spectrophotometry (Spectra Max 340PC) at 610 nm. Data were normalized with sample weight and data obtained from the liver.

FITC-Dextran Permeability Assay

Mice were given intracardiac injection with 200 μL of saline containing 2 μmol/L of lysine-fixable FITC-labeled dextran (FITC-D 2×10^6 molecular weight; Molecular Probes) for 5 min followed by 2 min of 0.05 mol/L citrate in 1% paraformaldehyde (pH 3.5) while under anesthesia. After sacrifice, tumors and livers were collected immediately and frozen using optimal cutting temperature compound. Five-micrometer-thick sections were prepared and mounted in VectaShield with 4′,6-diamidino-2-phenylindole (Vector Laboratories) followed by analysis with a confocal microscopy (Leica TCS SP2, Leica Microsytems).

Tetrazolium Salt 3-(4,5-dimethylthiazol-2-yl)-2,5-Diphenyltetrazolium Bromide Assay

TDEC were plated at the range of 1×10^3 to 2×10^3 cells/well into 96-well tissue culture plates (Corning Glass) and incubated at 37°C in a humidified atmosphere containing 5% CO_2. After 24 h post-plating, cells were either treated for 48 h with vehicle or varying doses of calcitriol. Cells were harvested by adding 20 μL of 0.5% 3-(4,5-dimethylthiazol-2-yl)-2,5-diphenyltetrazolium bromide (Sigma) for 3 h at 37°C. The medium was removed, and the cells were solubilized with 10% SDS/10 mmol/L HCl overnight at 37°C. The absorbance was read with an ELISA reader (Spectra Max 340PC) at 490 nm.

Western Blot Analysis

Twenty-four hours post-plating, the cells were treated with vehicle or 10 nmol/L of calcitriol. After 48 h, the cells were harvested and whole cell lysates were prepared using lysis buffer as described previously (9). For *in vivo* tumor and Matrigel plug specimens, protein lysates were prepared using CelLytic Lysis Buffer (Sigma). Protein samples (30 μg) were resolved by SDS-PAGE, and transferred overnight to polyvinylidene difluoride membranes. Western blot analysis was performed as previously described. Antibodies used include VDR (Santa Cruz Biotechnology), hypoxia-inducible factor-1α (HIF-1α; ABR), vascular endothelial growth factor (VEGF; Santa Cruz Biotechnology), VEGF receptor 2 (Cell Signaling), angiopoietin 1 (Ang1; U.S. Biologicals), Tie1 (Santa Cruz Biotechnology), Tie2 (Santa Cruz Biotechnology), platelet-derived growth factor-B (PDGF-B; Santa Cruz Biotechnology), PDGF receptor-β (Santa Cruz Biotechnology). Anti-rabbit and anti-mouse horseradish peroxidase–conjugated secondary antibodies were purchased from Amersham Life Sciences and actin was detected using the actin kit from Oncogene Research Products.

ELISA

Protein lysates were prepared from tumors using CelLytic Lysis Buffer (Sigma). All ELISA procedures were performed using ELISA development kits, murine VEGF (PeproTech, Inc.), murine HIF-1α (R&D Systems), murine Ang1 (R&D Systems), and murine PDGF-B (R&D Systems) following the instructions of the manufacturer. Data were collected from at least five samples from each group and were measured in triplicate.

24-Hydroxylase Promoter-Luciferase Reporter Assay

Cells were plated on 48-well plates and cultured for 24 h in 5% charcoal-stripped medium and then treated for 3 h with a constant dose of adenovirus containing β-galactosidase and adenovirus containing 24-hydroxylase promoter-luciferase construct or adenoviral empty vector control in serum-free medium. The cells were treated with varying doses of calcitriol for 48 h in 5% charcoal-stripped medium. Cells were harvested and cell lysates were obtained as described previously (9). The cell lysates were then subjected to Luciferase Assay Reagent (Promega) and the light produced was measured with a luminometer (Veritas Microplate Luminometer). β-Galactosidase activity was obtained using β-Galactosidase Enzyme Assay System (Promega) and the absorbance was measured with an ELISA reader (Spectra Max 340PC) at 520 nm. The relative luciferase unit was obtained by normalizing the luciferase unit with the activity of β-galactosidase and total protein from each lysate.

Cell Cycle Analysis

Endothelial cells were plated and treated at a final concentration 10 nmol/L of calcitriol. Cells were harvested 48 h after treatment by trypsinization, washed using PBS and fixed with 70% ethanol. The cells were RNase-treated prior to staining with 400 μL of 50 μg/mL propidium iodide (Sigma) in PBS solution, filtered through a 30 μm nylon mesh, and analyzed by flow cytometry using a BD FACScan. Cell cycle analysis was performed using ModFit software.

Statistical analysis. Differences between groups were analyzed for statistical significance using Student's *t* test (two-tailed). All data were

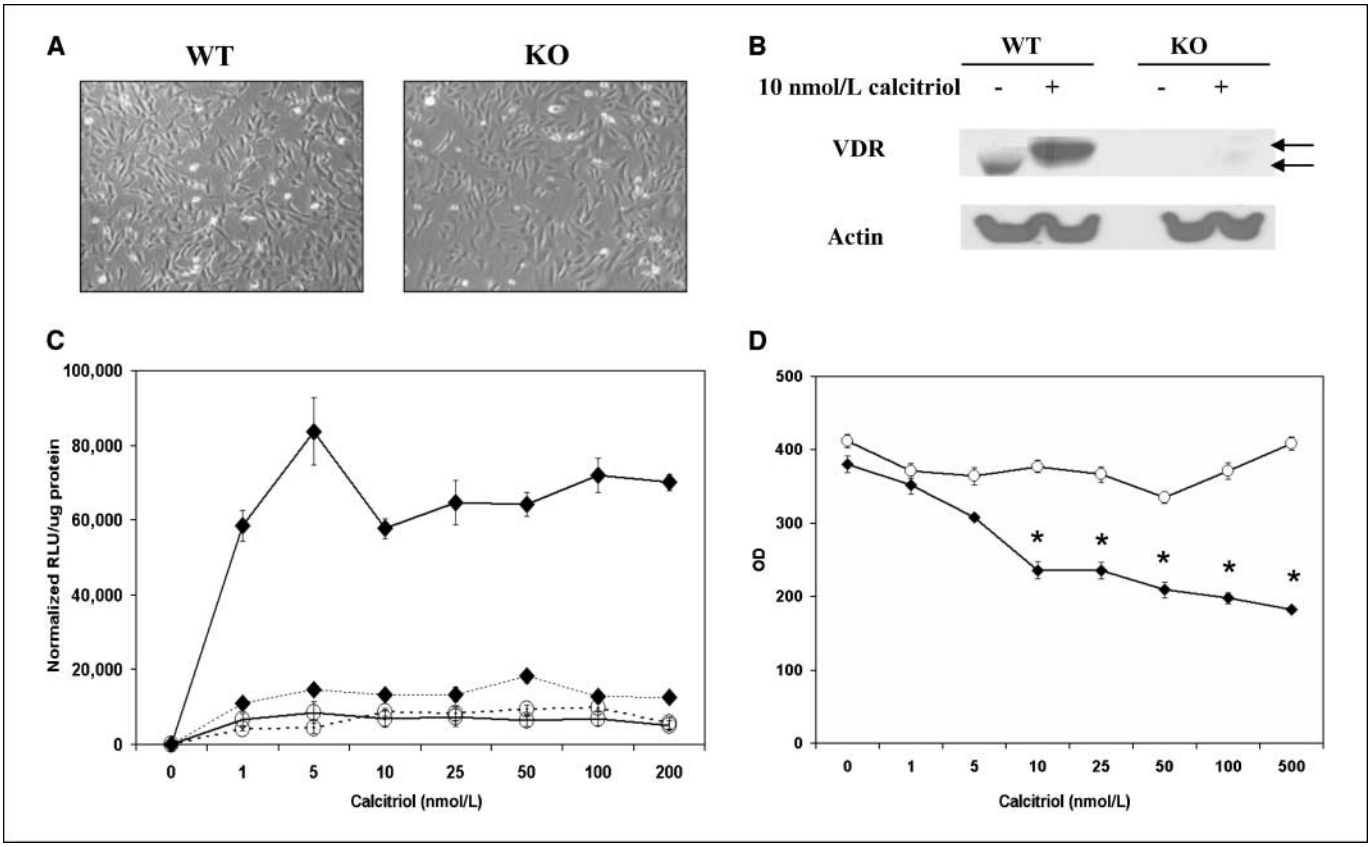

Figure 1. TDEC expressing VDR is more sensitive to the growth-inhibitory effects of calcitriol. *A,* phase contrast pictures showing no significant obvious difference in cell morphology of TDEC isolated from VDR WT or KO mice. *B,* VDR protein expression (*arrows*) was observed in 48-h calcitriol-treated TDEC isolated from VDR WT but not KO mice, as shown by Western blot analysis. *C,* transactivation activity of VDR is observed in TDEC expressing VDR (♦) but not in those from KO mice (○). TDEC were transfected with a constant dose of adenoviral 24-hydroxylase promoter luciferase reporter and adenoviral β-galactosidase expression vector for 3 h before treatment with vehicle (*dotted lines*) or 10 nmol/L calcitriol (*solid lines*) for 48 h. Luminescence data were normalized with β-galactosidase activities, and the empty adenoviral control vector showed minimal luciferase activity (data not shown). *D,* the effects of 48 h treatment of 1 to 500 nmol/L calcitriol on cell viability as measured by MTT assay. TDEC isolated from VDR WT (♦) but not those from KO mice (○) were responsive to the antiproliferative effects of calcitriol. *, $P < 0.001$ (Student's *t* test). *RLU*, relative luciferase unit. Representative of three independent experiments.

Table 1. Calcitriol treatment induces G_0/G_1 cell cycle arrest in TDEC expressing VDR

	WT			KO		
	G_1	S	G_2	G_1	S	G_2
Vehicle	45.5	53.1	1.4	42.3	49.5	8.2
Calcitriol (10 nmol/L)	76.9	23.1	0	36.2	50.0	13.8

NOTE: Propidium iodide staining using flow cytometry was performed with 48 h vehicle or 10 nmol/L calcitriol treated-TDEC from VDR WT and KO mice. Representative results of three independent experiments are shown.

expressed as the mean (with SD) of at least three determinants, unless stated otherwise.

Results

TDEC isolated from VDR KO mice are not sensitive to calcitriol-mediated growth inhibition. We showed that calcitriol exerts growth-inhibitory effects on TDEC by inducing G_0/G_1 cell cycle arrest and apoptosis (9). To determine the role of VDR on these effects, we isolated TDEC from TRAMP-2 tumors grown for 30 days in WT and KO mice, using methods previously described (29). As shown in Fig. 1*A*, there was no obvious difference in cell morphology of TDEC when isolated from different VDR genotype mice. The doubling time for each cell type was similar (data not shown). Upon treatment with calcitriol, VDR expression was induced in TDEC isolated from WT but not in those from KO mice (Fig. 1*B*). Using the 24-hydroxylase promoter-luciferase reporter, we showed that in TDEC expressing VDR, but not those from KO mice, calcitriol transactivated CYP24, a calcitriol-responsive gene (Fig. 1*C*). These results indicate that endothelial cells derived from TRAMP tumors grown in VDR KO mice were VDR negative and could not activate the VDR-mediated signaling pathway.

TDEC from these mice were treated with 0 to 500 nmol/L of calcitriol for 48 hours and cell viability was determined using the 3-(4,5-dimethylthiazol-2-yl)-2,5-diphenyltetrazolium bromide assay. TDEC expressing VDR were growth inhibited in a dose-dependent manner (Fig. 1*D*). However, in the absence of VDR, TDEC were minimally affected by similar treatment (Fig. 1*D*). The growth inhibition observed in TDEC expressing VDR was accompanied by an induction of G_0/G_1 cell cycle arrest, as measured by propidium iodide staining (Table 1). An increase of G_0/G_1 phase cells from 45% to 77% and a decrease of S phase cells from 53% to 23% were observed in calcitriol-treated TDEC from WT mice (Table 1). These effects were not observed in TDEC from KO mice. These results indicate that calcitriol-mediated growth inhibition in TDEC is a VDR-dependent event.

Vessels in TRAMP-2 tumors in VDR KO mice are enlarged and have lower pericyte coverage. Detailed examination of the tumor vascular morphology was performed by immunohistochemical staining of tumor sections for the endothelial cell marker, CD31. Although mean vessel density was not different between the two groups, vessel lumen size and percentage vessel area per field were higher in tumors of KO mice when compared with WT mice ($P < 0.001$; Table 2). Using CD31 and α-SMA (pericyte marker) double staining to measure pericyte coverage vessels in the tumor of VDR KO mice have less pericyte coverage when compared with those in WT mice (Fig. 2*B*). In WT mice, the average pericyte coverage of the vessels is 39%, whereas tumor vessels in KO mice have ~11% pericyte coverage (Table 2). These findings suggest a lower degree of vessel maturation in VDR KO vessels. In addition to the microvessels, there was also a proportion of enlarged vessels found in KO mice and these are not obvious in WT animals (Fig. 2*A*; Table 2).

Tumors in VDR WT and KO mice have different vascular properties and size. To evaluate the functional implications of these morphologic differences, we examined tumor perfusion using contrast-enhanced magnetic resonance imaging. Change in longitudinal relaxation rates (ΔR_1) of tumors implanted in WT and KO mice were plotted as a function of time and variables of vascular volume (*Y*-intercept) and permeability (slope) calculated. The vascular volume of TRAMP-C2 tumors implanted in KO mice (0.1953 ± 0.005) was significantly higher than tumors implanted in WT (0.1047 ± 0.0205; $P < 0.0001$; Fig. 3*A*). There was no difference in vascular permeability between the two types of tumors (Fig. 3*A*).

Table 2. Tumor vessels in VDR KO mice were enlarged with lower pericyte coverage

	Vessel lumen area (μm)	Vessel area per field (%)	No. of vessels per field	SMA positive (%)
WT	271.2 ± 440 ($n = 5$)	0.92 ± 0.87 ($n = 5$)	40.6 ± 12.7 ($n = 5$)	38.9 ± 22.9 ($n = 5$)
KO	$3{,}061.6 \pm 5{,}081$ ($n = 5$)*	23.5 ± 6.5 ($n = 5$)*	41.8 ± 16.6 ($n = 5$)	11 ± 16.8 ($n = 5$)*

NOTE: Vessel lumen size, percentage of vessel area/field, and vessel number/field in tumors were quantified from sections stained with endothelial marker CD31. Pericyte coverage or percentage of SMA was calculated from the overlapping area of CD31 and pericyte marker α-SMA to the total CD31 positive area in each field. *n*, number of animals.
*$P < 0.001$, compared with WT (Student's *t* test).

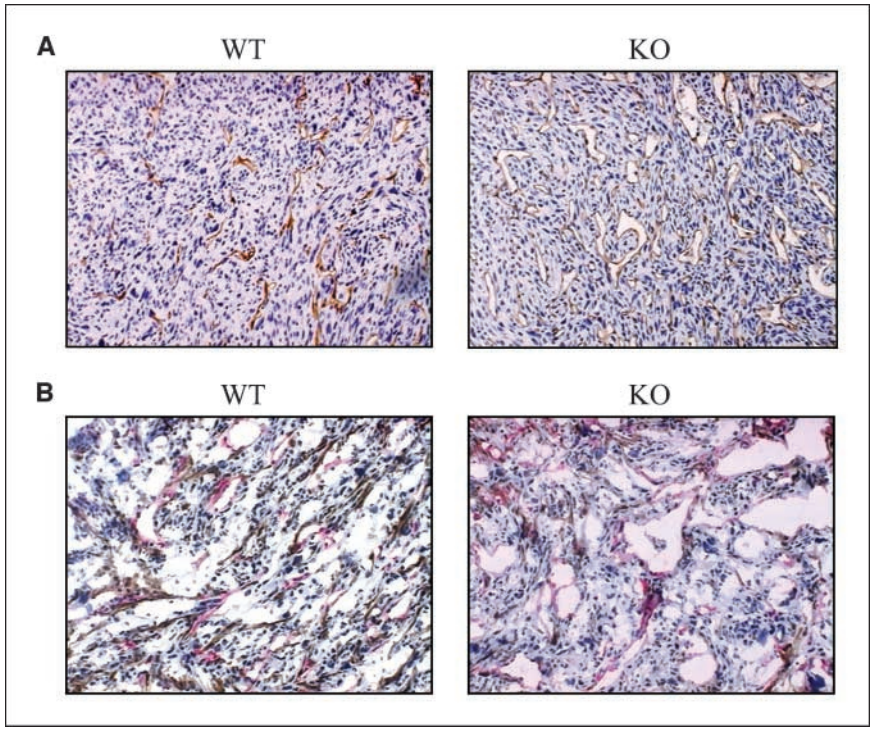

Figure 2. Enlargement of tumor vessels in TRAMP tumors in VDR KO mice is associated with lower pericyte coverage. *A,* representative of endothelial marker CD31–stained vessels (*brown*) found in tumors implanted in VDR WT and KO mice. Magnification, ×100. *B,* representative of endothelial marker CD31 (*pink*) and pericyte marker α-SMA (*brown*) positive vessels found in tumors in both VDR WT and KO mice. Magnification, ×100.

No significant change in the longitudinal relaxation rates was observed in kidneys and muscle tissues between VDR WT and VDR KO mice (data not shown).

We further evaluated vascular volume and permeability using quantitative *in vivo* Evans blue dye assay and qualitative FITC-dextran staining. Tumors from VDR KO mice showed a significantly higher Evans blue dye content (P = 0.029), indicating a higher vascular volume in these tumors (Fig. 3*B*). Confocal microscopy analysis of FITC-dextran–stained tumor vasculature showed a higher degree of plasma extravasation in KO versus WT animals (Fig. 3*C*). FITC-dextran–stained vasculature in the liver served as a control for injection of the dyes.

We compared the growth of TRAMP-C2 tumors in VDR WT and KO mice. Tumors were palpable around day 14 post-inoculation; subsequently, tumor measurement was performed twice a week (Fig. 3*D*). From day 18 to day 31, TRAMP-C2 tumors in KO mice were larger than those in WT animals (P = 0.018).

Abnormal tumor vasculature in VDR KO mice is associated with increased HIF-1α, VEGF, Ang1, and PDGF-B expression. Angiogenesis is a process governed by complex signaling pathways that promote endothelial cell proliferation and vascular maturation (25). To determine if the observed differences in angiogenesis between WT and KO tumors were related to dysregulation of angiogenic signaling pathways, we examined hypoxia-induced factor-1α (HIF-1α), VEGF, Ang1, and PDGF-B protein expression from the tumor lysates. Tumors from VDR KO mice exhibited a significantly higher level of HIF-1α protein when compared with WT mice (P = 0.01) as measured by ELISA (Fig. 4*A*). There was a significant increase in VEGF expression in tumors from KO mice when compared with WT (Fig. 4*B* and *E*). No significant change was observed in VEGF receptor 2 protein level between the two groups (Fig. 4*E*). Higher expression of Ang1 (Fig. 4*C* and *E*) and PDGF-BB (the dimer form) was also observed (Fig. 4*D* and *E*) in tumors from VDR KO mice as compared with the WT counterpart. No differences were observed in the expression of the receptors for Ang1 (Tie1 and Tie2) and PDGF-BB (PDGF-Rβ) between these tumors (Fig. 4*E*). Increased expression of these proangiogenic signaling molecules could, at least in part, account for the observed tumor vasculature characteristics in VDR KO mice.

Discussion

Calcitriol exerts profound antiproliferative effects on TDEC by inducing G_0/G_1 cell cycle arrest and apoptosis (8, 9). In TDEC, treatment with calcitriol up-regulates VDR protein expression and activates VDR signaling pathway (9). Using VDR KO mice, this study shows that VDR plays a major role in calcitriol-mediated antiproliferative effects in TDEC and in the development of tumor angiogenesis *in vivo*. TDEC isolated from tumors implanted in VDR WT, but not those from KO mice, showed enhanced VDR protein expression and are growth-inhibited by calcitriol. Calcitriol treatment induced G_0/G_1 cell cycle arrest in TDEC expressing VDR but not VDR KO TDEC. In calcitriol-treated TDEC from VDR KO mice, the lack of a luciferase signal from the promoter reporter assay suggests that calcitriol-activated VDR may be involved in regulating the transcription of various target genes governing cell growth (31).

The absence of VDR in tumor-infiltrating vessels results in a more aberrant vasculature. Compared with WT animals, the tumor vessels in the KO mice are enlarged, are associated with fewer pericytes and these tumors contain increased content of angiogenic factors such as HIF-1α, VEGF, Ang1, and PDGF-BB.

During rapid growth, tumor cells encounter hypoxic conditions which result in the induction of HIF-1α (32). HIF-1α can act as a transcriptional activator for various genes including VEGF (33). VEGF is a potent endothelial cell growth factor and survival molecule (34). Studies using transgenic VEGF mice and adenovirally mediated ectopic VEGF overexpression animal models revealed

that excessive amounts of VEGF can result in enlarged and highly permeable vascular beds (35, 36). Similarly, in mice overexpressing Ang1, vessels were also dramatically enlarged compared with the control mice (37, 38). Although Ang1 does not stimulate the proliferation of endothelial cells (39), Ang1 could induce endothelial migration, tube formation, sprouting, and survival following various apoptotic insults (40). Ang1 synergized with VEGF to activate phosphoinositide-3-kinase and Akt signaling to promote endothelial cell survival (41). Consistent with these studies, our observation of significantly enlarged tumor vessels in VDR KO mice may be attributed to the high level of VEGF and Ang1 within the tumor microenvironment.

Despite the high expression of VEGF observed in tumors of VDR KO mice, our studies did not reveal a significant increase in vascular permeability in these tumors. These findings could be explained by the Ang1 overexpression in these tumors because studies by others have shown that vessels stimulated by Ang1 are resistant to plasma leakage (38). When both VEGF and Ang1 were overexpressed at the same time, the leakage-resistance of the Ang1 phenotype seems to dominate (38, 42). Taken together, we conclude that complete loss of VDR signaling results in aberrant angiogenic signaling pathways in the tumor microenvironment.

We showed that tumor vessels in KO animals were covered with fewer pericytes when compared with those in WT animals.

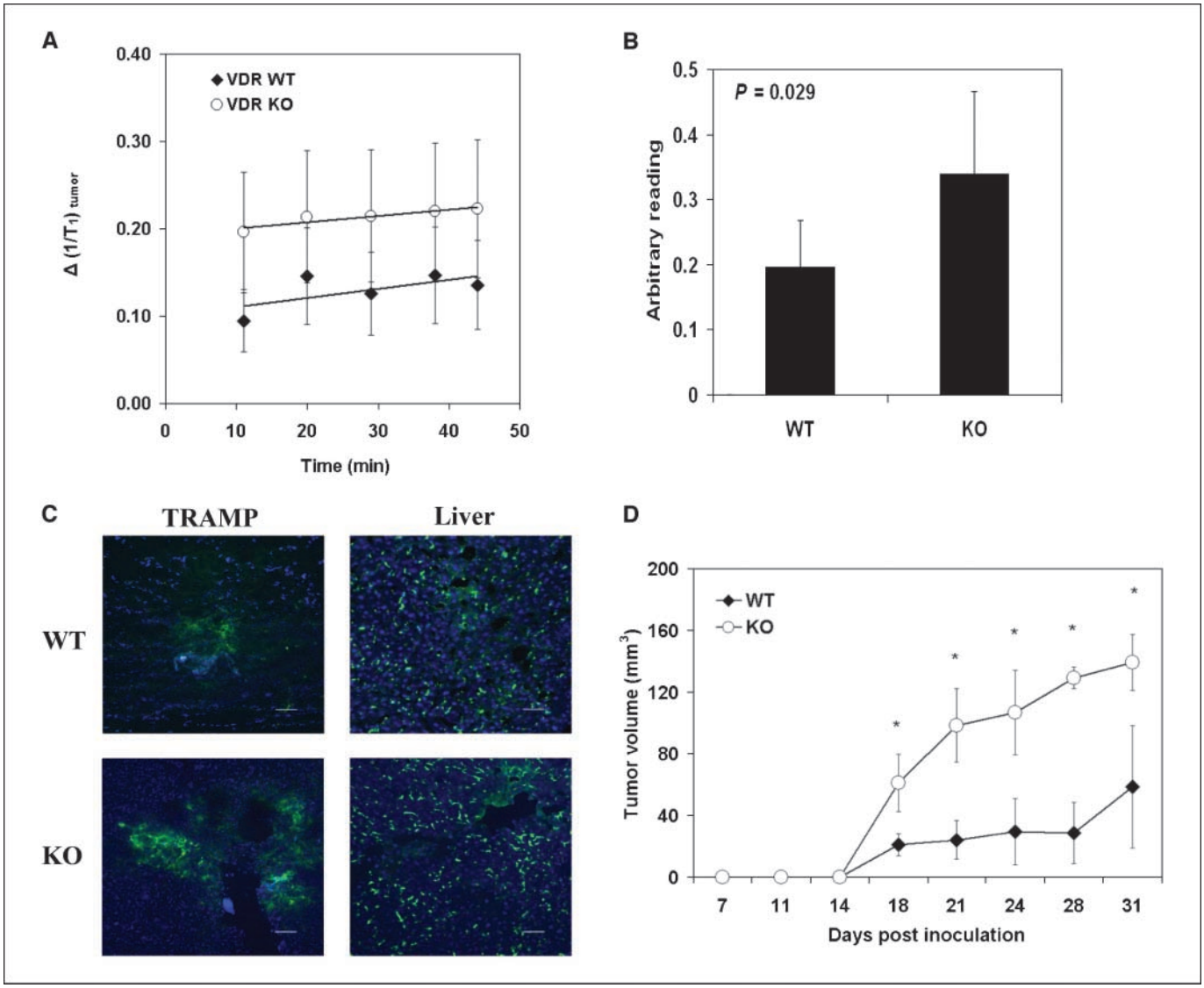

Figure 3. Difference in blood volume, vascular leakiness, and tumor size of tumors in VDR WT and KO mice. *A,* change in T1 relaxation rates (ΔR_1) over time of TRAMP tumors in VDR WT (♦) and KO (○) mice. Vascular volume and permeability values were calculated from ΔR_1 using linear regression analysis. Analysis of the slopes showed a slight, but not significant difference in permeability between the two groups. Significant differences were seen between the vascular volumes (*Y*-intercept) of tumors in VDR WT and KO mice ($P < 0.001$). *B,* modified *in vivo* Evans blue dye assay showed a significant increase in Evans blue dye content in tumors from VDR KO compared to WT. Animals were given 0.2 mL of 0.5% Evans blue intracardiacally under anesthesia for 5 min before being sacrificed. The dye from tumors was extracted using formamide, and readings were normalized with those from the livers. Data shown were from at least three to five animals per group. *C,* confocal microscopy analysis shows a more extensive leakage of FITC-dextran from the tumor vasculature in VDR KO than in WT animals. Animals were given 0.2 mL of 2 μmol/L FITC-dextran in saline intracardically before fixation with paraformaldehyde. Livers were used as a control for sufficient systemic delivery of the dye. Data shown were representative of three independent experiments. *Scale bar,* 200 μm. *D,* tumors in VDR KO mice were larger than those in WT mice. TRAMP cells (2×10^6) were implanted subcutaneously into VDR WT (♦) and KO (○) mice. The growth of the tumors, as measured by the tumor size, was monitored over time. There were at least 4 to 6 animals per group, and the data shown is representative of two independent experiments.

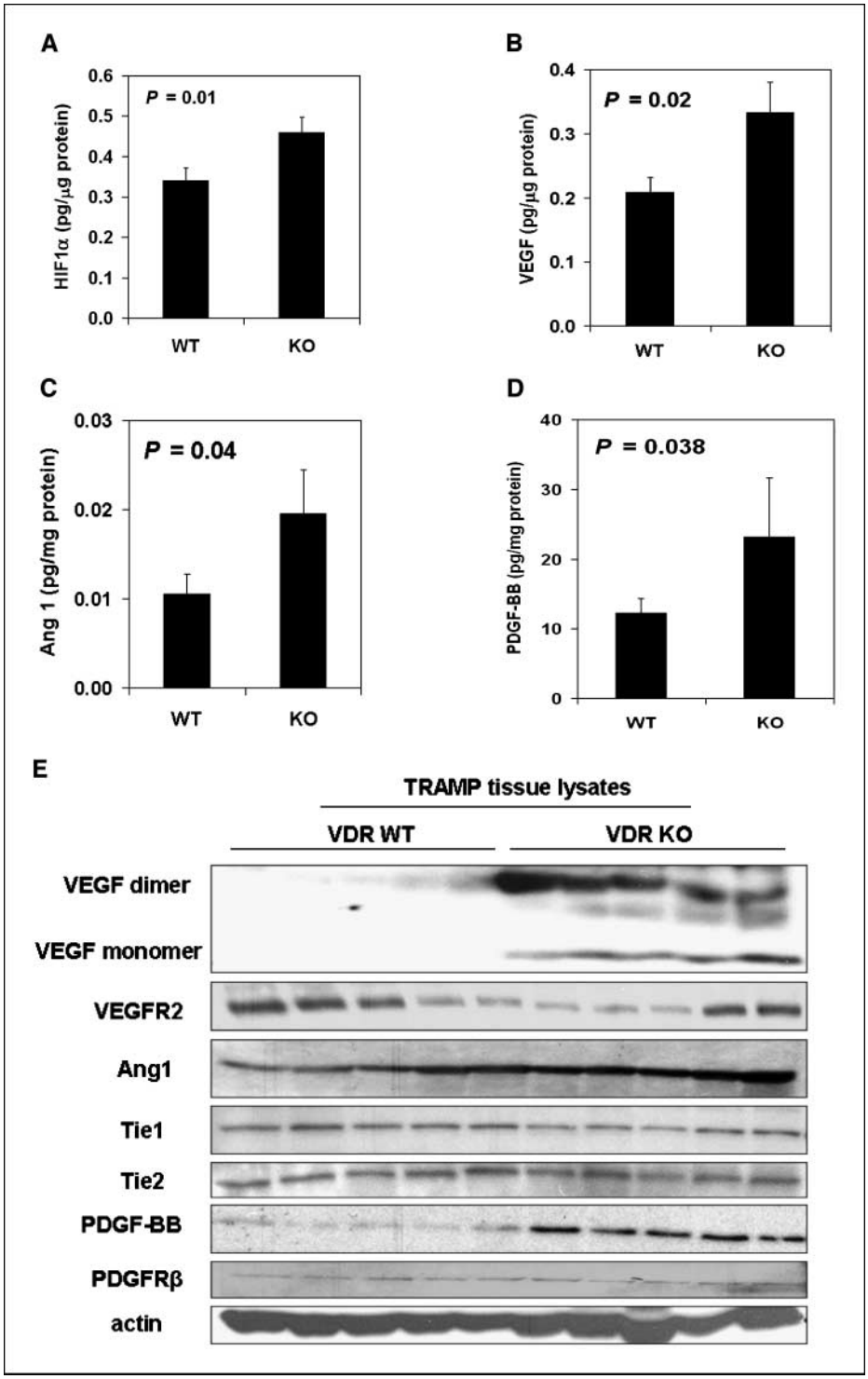

Figure 4. Abnormal vasculature in tumors from VDR KO mice is associated with increased HIF-1α, VEGF, angiopoietin 1, and PDGF-BB expression. *A* to *D,* tumor extracts were subjected to ELISA analyses for (*A*) HIF-1α, (*B*) VEGF, (*C*) Ang 1, and (*D*) PDGF-BB and the quantification of the growth factors was normalized with total protein. Data are from at least five tumors per group and statistical analyses were performed using Student's *t* test. *E,* representative of three experiments showing increased protein expression of VEGF, Ang1, and PDGF-BB in five individual tumors from KO mice compared with WT using Western blot analysis. No significant change in the expression of the respective receptors in both groups. *HIF1*, hypoxia-induced factor; *VEGF*, vascular endothelial growth factor; *Ang1*, angiopoietin-1; *PDGF-BB*, platelet-derived growth factor-BB; *PDGFR*, platelet-derived growth factor receptor.

Pericytes regulate endothelial cell proliferation, survival, migration, and differentiation, and also modulate blood flow and vascular permeability. It has been shown that lack of pericyte coverage may represent a window of plasticity for further vessel remodeling (43). Therefore, the vessels in VDR KO mice may be more responsive to mitogenic and survival signals. However, the lower pericyte coverage observed in VDR KO mice is contrary to the increase of the pericyte-recruiting factor, PDGF-BB expression, in these tumors. It has been shown that endothelial cells secrete PDGF-BB, which promotes pericyte recruitment in a paracrine fashion (43). Interestingly, ectopic PDGF-BB expression could disrupt endothelial-pericyte interactions and may lead to abnormalities in pericyte attachment and in vessel remodeling (43). In addition to promoting pericyte recruitment, PDGF-BB induces intratumoral lymphangiogenesis and lymphatic metastasis in the murine fibrosarcoma model (44), promotes angiogenesis and glial tumorigenesis (45), and directly promotes the growth of prostate cancer cells (46). *In vitro* and *in vivo* studies show that targeting this

signaling pathway using PDGF receptor tyrosine kinase inhibitors (such as STI571), can enhance paclitaxel-mediated regression of prostate tumors (47). Therefore, the enhanced PDGF-BB expression within the TRAMP-C2 tumors in VDR KO mice may not only affect pericyte recruitment but might also lead to increased neovascularization and tumor cell growth.

The role of VDR signaling in regulating these angiogenic pathways is not well characterized. In various human cancer cells, calcitriol inhibits HIF-1α protein expression and HIF-1α target genes such as VEGF, endothelin-1, and glucose transporter-1 (48). Furthermore, there are DR3 type vitamin D response element–like sequences in the promoter region of the rat VEGF gene (48); therefore, it is possible that calcitriol modulates VEGF expression at the transcriptional level (49, 50). Whether Ang1 and PDGF-B expression are also regulated through direct VDR-DNA interaction remains to be elucidated. In calcitriol-treated TDEC WT cells, we observed a reduction of VEGF, Ang1, and PDGF-BB expression but this was not seen in TDEC KO cells. This model of TDEC, isolated from different tumor microenvironments, will allow for a direct examination of the role of VDR in mediating the effects of calcitriol on angiogenic signaling pathways.

Our studies also contribute to the increasing evidence indicating that host cells contribute to tumor growth. In addition to the endothelial cells, there are other host cells present in the tumor microenvironment, e.g., pericytes, stromal cells, and immune cells. The role of VDR signaling in the interactions among these cell types and tumor cells in tumorigenesis remains to be elucidated. In this model, we compared vasculature from the same tumor cells grown in different VDR genetic backgrounds. The differences of phenotype observed could be directly attributed to the VDR activity in the host cells. Our studies provide *in vivo* molecular evidence that calcitriol-VDR signaling has a substantial effect on tumor angiogenesis and is required for the growth-inhibitory effects on TDEC.

Disclosure of Potential Conflicts of Interest

No potential conflicts of interest were disclosed.

Acknowledgments

Received 6/20/2008; revised 9/3/2008; accepted 9/23/2008.

Grant support: NIH/NCI CA67267, CA85142, and CA95045 and DOD grant PCRP050202.

The costs of publication of this article were defrayed in part by the payment of page charges. This article must therefore be hereby marked *advertisement* in accordance with 18 U.S.C. Section 1734 solely to indicate this fact.

We thank Harold Dvorak, Mohamed Khan, Shaozeng Zhang, and Arup Bhattacharya for discussion, and Marie Demay for providing the VDR KO mice colony. We are also grateful to Sandra Buitrago and the rest of the RPCI Department of Laboratory Animal Resource for assistance in animal husbandry, and Mary Vaughan and Histology Laboratory Services staff for immunohistochemical support.

References

1. van den Bemd GJ, Pols HA, van Leeuwen JP. Antitumor effects of 1,25-dihydroxyvitamin D3 and vitamin D analogs. Curr Pharm Des 2000;6:717–32.
2. Johnson CS, Muindi JR, Hershberger PA, Trump DL. The antitumor efficacy of calcitriol: preclinical studies. Anticancer Res 2006;26:2543–9.
3. Koeffler HP, Hirji K, Itri L. 1,25-Dihydroxyvitamin D3: *in vivo* and *in vitro* effects on human preleukemic and leukemic cells. Cancer Treat Rep 1985;69:1399–407.
4. Hershberger PA, Modzelewski RA, Shurin ZR, Rueger RM, Trump DL, Johnson CS. 1,25-Dihydroxycholecalciferol (1,25-D3) inhibits the growth of squamous cell carcinoma and down-modulates p21(Waf1/Cip1) *in vitro* and *in vivo*. Cancer Res 1999;59:2644–9.
5. Lokeshwar BL, Schwartz GG, Selzer MG, et al. Inhibition of prostate cancer metastasis *in vivo*: a comparison of 1,23-dihydroxyvitamin D (calcitriol) and EB1089. Cancer Epidemiol Biomarkers Prev 1999;8:241–8.
6. Welsh J. Vitamin D and breast cancer: insights from animal models. Am J Clin Nutr 2004;80:1721–4S.
7. Diaz GD, Paraskeva C, Thomas MG, Binderup L, Hague A. Apoptosis is induced by the active metabolite of vitamin D3 and its analogue EB1089 in colorectal adenoma and carcinoma cells: possible implications for prevention and therapy. Cancer Res 2000;60:2304–12.
8. Bernardi RJ, Johnson CS, Modzelewski RA, Trump DL. Antiproliferative effects of 1α,25-dihydroxyvitamin D(3) and vitamin D analogs on tumor-derived endothelial cells. Endocrinology 2002;143:2508–14.
9. Chung I, Wong MK, Flynn G, Yu WD, Johnson CS, Trump DL. Differential antiproliferative effects of calcitriol on tumor-derived and matrigel-derived endothelial cells. Cancer Res 2006;66:8565–73.
10. Flynn G, Chung I, Yu WD, et al. Calcitriol (1,25-Dihydroxycholecalciferol) selectively inhibits proliferation of freshly isolated tumor-derived endothelial cells and induces apoptosis. Oncology 2007;70:447–57.
11. Li YC, Pirro AE, Amling M, et al. Targeted ablation of the vitamin D receptor: an animal model of vitamin D-dependent rickets type II with alopecia. Proc Natl Acad Sci U S A 1997;94:9831–5.
12. Merke J, Milde P, Lewicka S, et al. Identification and regulation of 1,25-dihydroxyvitamin D3 receptor activity and biosynthesis of 1,25-dihydroxyvitamin D3. Studies in cultured bovine aortic endothelial cells and human dermal capillaries. J Clin Invest 1989;83:1903–15.
13. Chung I, Karpf AR, Muindi JR, et al. Epigenetic silencing of CYP24 in tumor-derived endothelial cells contributes to selective growth inhibition by calcitriol. J Biol Chem 2007;282:8704–14.
14. Christakos S, Raval-Pandya M, Wernyj RP, Yang W. Genomic mechanisms involved in the pleiotropic actions of 1,25-dihydroxyvitamin D3. Biochem J 1996;316:361–71.
15. Dostal LA, Toverud SU. Effect of vitamin D3 on duodenal calcium absorption *in vivo* during early development. Am J Physiol 1984;246:G528–34.
16. Halloran BP, DeLuca HF. Effect of vitamin D deficiency on fertility and reproductive capacity in the female rat. J Nutr 1980;110:1573–80.
17. Mathews CH, Brommage R, DeLuca HF. Role of vitamin D in neonatal skeletal development in rats. Am J Physiol 1986;250:E725–30.
18. Balsan S, Garabedian M, Larchet M, et al. Long-term nocturnal calcium infusions can cure rickets and promote normal mineralization in hereditary resistance to 1,25-dihydroxyvitamin D. J Clin Invest 1986;77:1661–7.
19. Beer S, Tieder M, Kohelet D, et al. Vitamin D resistant rickets with alopecia: a form of end organ resistance to 1,25 dihydroxy vitamin D. Clin Endocrinol (Oxf) 1981;14:395–402.
20. Malloy PJ, Pike JW, Feldman D. Hereditary 1,25-dihydroxyvitamin D resistant rickets. In: Feldman D, Pike JW, Glorieux FH, editors. Vitamin D. New York: Elsevier Academic Press; 2005. p. 1207–38.
21. Yoshizawa T, Handa Y, Uematsu Y, et al. Mice lacking the vitamin D receptor exhibit impaired bone formation, uterine hypoplasia and growth retardation after weaning. Nat Genet 1997;16:391–6.
22. Van Cromphaut SJ, Dewerchin M, Hoenderop JG, et al. Duodenal calcium absorption in vitamin D receptor-knockout mice: functional and molecular aspects. Proc Natl Acad Sci U S A 2001;98:13324–9.
23. Erben RG, Soegiarto DW, Weber K, et al. Deletion of deoxyribonucleic acid binding domain of the vitamin D receptor abrogates genomic and nongenomic functions of vitamin D. Mol Endocrinol 2002;16:1524–37.
24. Zinser GM, Sundberg JP, Welsh J. Vitamin D(3) receptor ablation sensitizes skin to chemically induced tumorigenesis. Carcinogenesis 2002;23:2103–9.
25. Folkman J. Tumor angiogenesis: therapeutic implications. N Engl J Med 1971;285:1182–6.
26. Rafii S, Avecilla S, Shmelkov S, et al. Angiogenic factors reconstitute hematopoiesis by recruiting stem cells from bone marrow microenvironment. Ann N Y Acad Sci 2003;996:49–60.
27. Seshadri M, Mazurchuk R, Spernyak JA, Bhattacharya A, Rustum YM, Bellnier DA. Activity of the vascular-disrupting agent 5,6-dimethylxanthenone-4-acetic acid against human head and neck carcinoma xenografts. Neoplasia 2006;8:534–42.
28. Li YC, Amling M, Pirro AE, et al. Normalization of mineral ion homeostasis by dietary means prevents hyperparathyroidism, rickets, and osteomalacia, but not alopecia in vitamin D receptor-ablated mice. Endocrinology 1998;139:4391–6.
29. Foster BA, Gingrich JR, Kwon ED, Madias C, Greenberg NM. Characterization of prostatic epithelial cell lines derived from transgenic adenocarcinoma of the mouse prostate (TRAMP) model. Cancer Res 1997;57:3325–30.
30. Modzelewski RA, Davies P, Watkins SC, Auerbach R, Chang MJ, Johnson CS. Isolation and identification of fresh tumor-derived endothelial cells from a murine RIF-1 fibrosarcoma. Cancer Res 1994;54:336–9.
31. White JH. Profiling 1,25-dihydroxyvitamin D3-regulated gene expression by microarray analysis. J Steroid Biochem Mol Biol 2004;89–90:239–44.
32. Gordan JD, Simon MC. Hypoxia-inducible factors: central regulators of the tumor phenotype. Curr Opin Genet Dev 2007;17:71–7.
33. Mabjeesh NJ, Amir S. Hypoxia-inducible factor (HIF) in human tumorigenesis. Histol Histopathol 2007;22:559–72.
34. Ferrara N. VEGF and the quest for tumour angiogenesis factors. Nat Rev Cancer 2002;2:795–803.
35. Nagy JA, Feng D, Vasile E, et al. Permeability properties of tumor surrogate blood vessels induced by VEGF-A. Lab Invest 2006;86:767–80.
36. Thurston G, Suri C, Smith K, et al. Leakage-resistant blood vessels in mice transgenically overexpressing angiopoietin-1. Science 1999;286:2511–4.

37. Thurston G, Wang Q, Baffert F, et al. Angiopoietin 1 causes vessel enlargement, without angiogenic sprouting, during a critical developmental period. Development 2005;132:3317–26.
38. Suri C, McClain J, Thurston G, et al. Increased vascularization in mice overexpressing angiopoietin-1. Science 1998;282:468–71.
39. Davis S, Aldrich TH, Jones PF, et al. Isolation of angiopoietin-1, a ligand for the TIE2 receptor, by secretion-trap expression cloning. Cell 1996;87:1161–9.
40. Metheny-Barlow LJ, Li LY. The enigmatic role of angiopoietin-1 in tumor angiogenesis. Cell Res 2003;13:309–17.
41. Benjamin LE. The controls of microvascular survival. Cancer Metastasis Rev 2000;19:75–81.
42. Thurston G. Complementary actions of VEGF and angiopoietins on blood vessel permeability and growth in mice. J Anat 2002;200:529.
43. Benjamin LE, Hemo I, Keshet E. A plasticity window for blood vessel remodelling is defined by pericyte coverage of the preformed endothelial network and is regulated by PDGF-B and VEGF. Development 1998;125:1591–8.
44. Cao R, Bjorndahl MA, Religa P, et al. PDGF-BB induces intratumoral lymphangiogenesis and promotes lymphatic metastasis. Cancer Cell 2004;6:333–45.
45. Shih AH, Holland EC. Platelet-derived growth factor (PDGF) and glial tumorigenesis. Cancer Lett 2006;232:139–47.
46. Nazarova N, Golovko O, Blauer M, Tuohimaa P. Calcitriol inhibits growth response to platelet-derived growth factor-BB in human prostate cells. J Steroid Biochem Mol Biol 2005;94:189–96.
47. Uehara H, Kim SJ, Karashima T, et al. Effects of blocking platelet-derived growth factor-receptor signaling in a mouse model of experimental prostate cancer bone metastases. J Natl Cancer Inst 2003;95:458–70.
48. Ben-Shoshan M, Amir S, Dang DT, Dang LH, Weisman Y, Mabjeesh NJ. 1α,25-dihydroxyvitamin D3 (Calcitriol) inhibits hypoxia-inducible factor-1/vascular endothelial growth factor pathway in human cancer cells. Mol Cancer Ther 2007;6:1433–9.
49. Haussler MR, Whitfield GK, Haussler CA, et al. The nuclear vitamin D receptor: biological and molecular regulatory properties revealed. J Bone Miner Res 1998;13:325–49.
50. Mantell DJ, Owens PE, Bundred NJ, Mawer EB, Canfield AE. 1α,25-dihydroxyvitamin D(3) inhibits angiogenesis *in vitro* and *in vivo*. Circ Res 2000;87:214–20.